Dysbindin is a potent inducer of RhoA–SRF-mediated cardiomyocyte hypertrophy

Ashraf Yusuf Rangrez,[1,3] Alexander Bernt,[1,3] Reza Poyanmehr,[1] Violetta Harazin,[1] Inka Boomgaarden,[1] Christian Kuhn,[1] Astrid Rohrbeck,[2] Derk Frank,[1,3] and Norbert Frey[1,3]

[1]Department of Internal Medicine III, University Medical Center Schleswig-Holstein, D-24105 Kiel, Germany
[2]Institute of Toxicology, Hannover Medical School, D-30625 Hannover, Germany
[3]German Centre for Cardiovascular Research, partner site Hamburg/Kiel/Lübeck, D-24105 Kiel, Germany

Dysbindin is an established schizophrenia susceptibility gene thoroughly studied in the context of the brain. We have previously shown through a yeast two-hybrid screen that it is also a cardiac binding partner of the intercalated disc protein Myozap. Because Dysbindin is highly expressed in the heart, we aimed here at deciphering its cardiac function. Using a serum response factor (SRF) response element reporter-driven luciferase assay, we identified a robust activation of SRF signaling by Dysbindin overexpression that was associated with significant up-regulation of SRF gene targets, such as Acta1 and Actc1. Concurrently, we identified RhoA as a novel binding partner of Dysbindin. Further phenotypic and mechanistic characterization revealed that Dysbindin induced cardiac hypertrophy via RhoA–SRF and MEK1–ERK1 signaling pathways. In conclusion, we show a novel cardiac role of Dysbindin in the activation of RhoA–SRF and MEK1–ERK1 signaling pathways and in the induction of cardiac hypertrophy. Future in vivo studies should examine the significance of Dysbindin in cardiomyopathy.

Introduction

In a previous effort to identify proteins involved in cardiomyocyte signal transduction, Myozap (Myocardium-enriched zonula occludens-1–associated protein) was discovered as a novel protein, which is localized to the intercalated disc (ID; Seeger et al., 2010). Myozap is a highly conserved, developmentally regulated cardiac protein (Seeger et al., 2010). Recently, Myozap has also been identified as a component of the cytoplasmic plaques of composite junctions and also localizing to the epithelial cell junctions (Rickelt et al., 2011; Pieperhoff et al., 2012). Knockdown of the *Myozap* orthologue in Zebrafish resulted in cardiomyopathy with severe contractile dysfunction (Seeger et al., 2010). Moreover, functional characterization revealed that Myozap promotes Rho-dependent serum response factor (SRF) signaling, whereas a newly identified Myozap binding partner, myosin phosphatase-RhoA–interacting protein (MRIP), inhibits this pathway (Seeger et al., 2010).

SRF is a multifunctional transcription factor, a founding member of the MADS box family of transcription factors, which regulate the expression of a variety of genes by binding to a specific promoter sequence known as CarG box (Shore and Sharrocks, 1995; Miano, 2010; Kuwahara and Nakao, 2011). SRF modulates the expression of a significant subset of cardiac-specific genes both during embryonic development and in the context of cardiac disease. For example, cardiac-specific overexpression of SRF in the postnatal heart leads to hypertrophic cardiomyopathy with increased fetal cardiac gene expression (Zhang et al., 2001a,b). On the other hand, targeted deletion of SRF in the developing heart results in lethal cardiac defects with reduced expression of several cardiac-specific genes (Miano et al., 2004; Parlakian et al., 2004). Likewise, disruption of SRF in the adult heart using a heart-specific Tamoxifen-inducible Cre recombinase induces dilated cardiomyopathy (Parlakian et al., 2005). By using both knockdown and overexpression approaches, Nelson et al. (2005) demonstrated that SRF is required for the induction of atrial natriuretic factor (or *Nppa* [*natriuretic peptide A*]), c-Fos, NCX1, brain natriuretic peptide

Correspondence to Norbert Frey: norbert.frey@uk-sh.de; or Derk Frank: derk.frank@uk-sh.de

Abbreviations used in this paper: ANOVA, analysis of variance; ARVCM, adult rat ventricular cardiomyocyte; co-IP, coimmunoprecipitation; ET, endothelin-1; ID, intercalated disc; KO, knockout; MRIP, myosin phosphatase-RhoA–interacting protein; NRVCM, neonatal rat ventricular cardiomyocyte; PE, phenylephrine; PVDF, polyvinylidene fluoride; qRT-PCR, quantitative real-time PCR; SRF, serum response factor; SRF-RE, SRF response element; Y2H, yeast two-hybrid.

The Rockefeller University Press $30.00
J. Cell Biol. Vol. 203 No. 4 643–656
www.jcb.org/cgi/doi/10.1083/jcb.201303052

(or *Nppb* [*natriuretic peptide B*]), α-actin, and α- and β-myosin heavy chain genes. Collectively, these in vitro and in vivo data suggest that SRF is crucial for the regulation and induction of genes associated with the progression of pathological cardiac hypertrophy and dilated cardiomyopathy. Nevertheless, cardiac hypertrophy is a complex process involving distinct yet interconnected mechanistic pathways comprised of several kinases, phosphatases, and transcription factors (Frey and Olson, 2003; Wilkins et al., 2004; Sanna et al., 2005; Heineke and Molkentin, 2006).

Dysbindin (dystrobrevin-binding protein) is ubiquitously expressed in various tissues and thus far been studied in neurons because of its association with the neurological disorder schizophrenia (Schwab et al., 2003; Bray et al., 2005; Talbot et al., 2011). Here, we present Dysbindin as a novel and unexpected binding partner of the cardiac protein Myozap. The Myozap–Dysbindin interaction is confirmed by coimmunoprecipitation (co-IP), and the binding region is mapped to the coiled-coil domain of Dysbindin. We found that Dysbindin is differentially expressed in several in vivo models of hypertrophy and cardiomyopathy. Of note, overexpression of Dysbindin robustly induces cardiomyocyte hypertrophy. Moreover, we identified RhoA, a small GTPase, as a novel binding partner of Dysbindin. Mechanistically, Dysbindin induces RhoA-dependent SRF signaling and downstream gene expression. Conversely, knockdown of Dysbindin results in inhibition of hypertrophic effects of a prohypertrophic agent, phenylephrine (PE), and endothelin-1 (ET). Collectively, our experiments identify a new role for Dysbindin in cardiomyocytes and imply a potential function in the pathogenesis of cardiac hypertrophy and failure.

Results

Dysbindin interacts with Myozap

Our group has recently discovered Myozap as a novel cardiac ID protein (Seeger et al., 2010). A yeast two-hybrid (Y2H) screen to determine cardiac-specific binding partners of Myozap unfolded Dysbindin as one of the potential interaction partners. The interaction was further confirmed by co-IP (Fig. 1 A). Secondary structure prediction of Dysbindin revealed that it contains a coiled-coil domain and a conserved Dysbindin domain. To map the exact site for this interaction, we cloned different fragments of Dysbindin as shown in Fig. 1 B and performed several co-IP experiments with Myozap. Fig. 1 C shows that the coiled-coil domain of Dysbindin is solely responsible for the interaction with Myozap.

Next, we determined the tissue distribution of Dysbindin expression in mouse and confirmed significant expression in the heart as well as in various other tissues (Fig. S1, A and B). At the protein level, Dysbindin showed highest expression in the brain (Fig. S1 A); however, its gene expression was relatively higher in the heart as determined by quantitative real-time PCR (qRT-PCR; Fig. S1 B).

Dysbindin localizes to the cytoplasm in other cell types; however, its subcellular localization in cardiomyocytes has not been reported yet. We used neonatal rat ventricular cardiomyocytes (NRVCMs), untreated or treated either with PE or with ET, and adult rat ventricular cardiomyocytes (ARVCMs) to study the precise localization of Dysbindin. Both cell types were coimmunostained with anti-Dysbindin and anti-Myozap antibodies. Isolated NRVCMs exhibited a prominent nuclear and scattered cytoplasmic localization of Dysbindin (Fig. 1 D, top), which was also observed in ARVCMs (Fig. S1 C). Myozap on the other hand was distinctly located at membrane and sparingly in cytosol (Fig. 1 D, top; and Fig. S1 C). However, upon PE/ET treatment, Dysbindin redistributed to the cellular membrane, colocalizing with Myozap (Fig. 1 D, middle and bottom).

Overexpression of Dysbindin induces SRF signaling in cardiomyocytes

We have reported earlier that Myozap activates Rho-dependent SRF signaling (Seeger et al., 2010). To explore the effect of Dysbindin in this pathway, we overexpressed Dysbindin (Fig. S2 A) in the absence or presence of Myozap in NRVCMs and assessed the activation of SRF signaling using SRF response element (SRF-RE) reporter luciferase assays. Interestingly, Dysbindin robustly activated SRF signaling, approximately eight- to tenfold, even to a higher extent than Myozap alone (approximately two- to threefold; Fig. 2 A). Coexpression of Dysbindin with Myozap exhibited an additive effect on SRF signaling (Fig. 2 A). We performed the assay using two control viruses (Ad [adenovirus]-LacZ and Ad-GFP) to reassure the findings (Fig. S2, B and C). Additionally, Myozap- and Dysbindin-mediated activation of SRF signaling was also observed in another mouse muscle cell line, C2C12 cells, supplementing the NRVCM data (Fig. S2 D). Furthermore, we also determined the expression levels of endogenous cardiac SRF targets in Dysbindin-overexpressing NRVCMs. We found an approximately two- to fourfold increase in the expression of smooth muscle α-actin (*acta1*) and cardiac muscle α-actin (*actc1*), whereas myosin heavy chain 7 (*myh7*) was significantly down-regulated (Fig. 2 B).

Next, we asked whether down-regulation of endogenous Dysbindin has an impact on Myozap-mediated SRF signaling. We therefore knocked down the expression of Dysbindin using siRNA (Fig. S2, E and F). Scrambled, unrelated siRNA was used as a control. Interestingly, siRNA-mediated knockdown of Dysbindin significantly reduced the activation of SRF-RE–luciferase reporter already at basal level (Fig. 2 C and Fig. S2 G). Similarly, down-regulation of Dysbindin repressed the Myozap-induced activation of SRF signaling (Fig. 2 C and Fig. S2 G), suggesting an important role of Dysbindin in Myozap-mediated activation of SRF signaling. Additionally, knockdown of Dysbindin reduced the expression of SRF targets, such as *acta1*, *actc1*, and *myl2* (*myosin light chain 2*), by 40–50% (Fig. 2 D).

RhoA is a novel binding partner of Dysbindin

To further dissect the role of Dysbindin in cardiomyocyte signaling, we performed a Y2H screen using human Dysbindin as bait against human cardiac cDNA library–derived prays. Interestingly, we identified RhoA as one of the novel interaction partners for Dysbindin in the screen, which we further validated in a pairwise Y2H binding assay (Fig. 3 A). We confirmed the

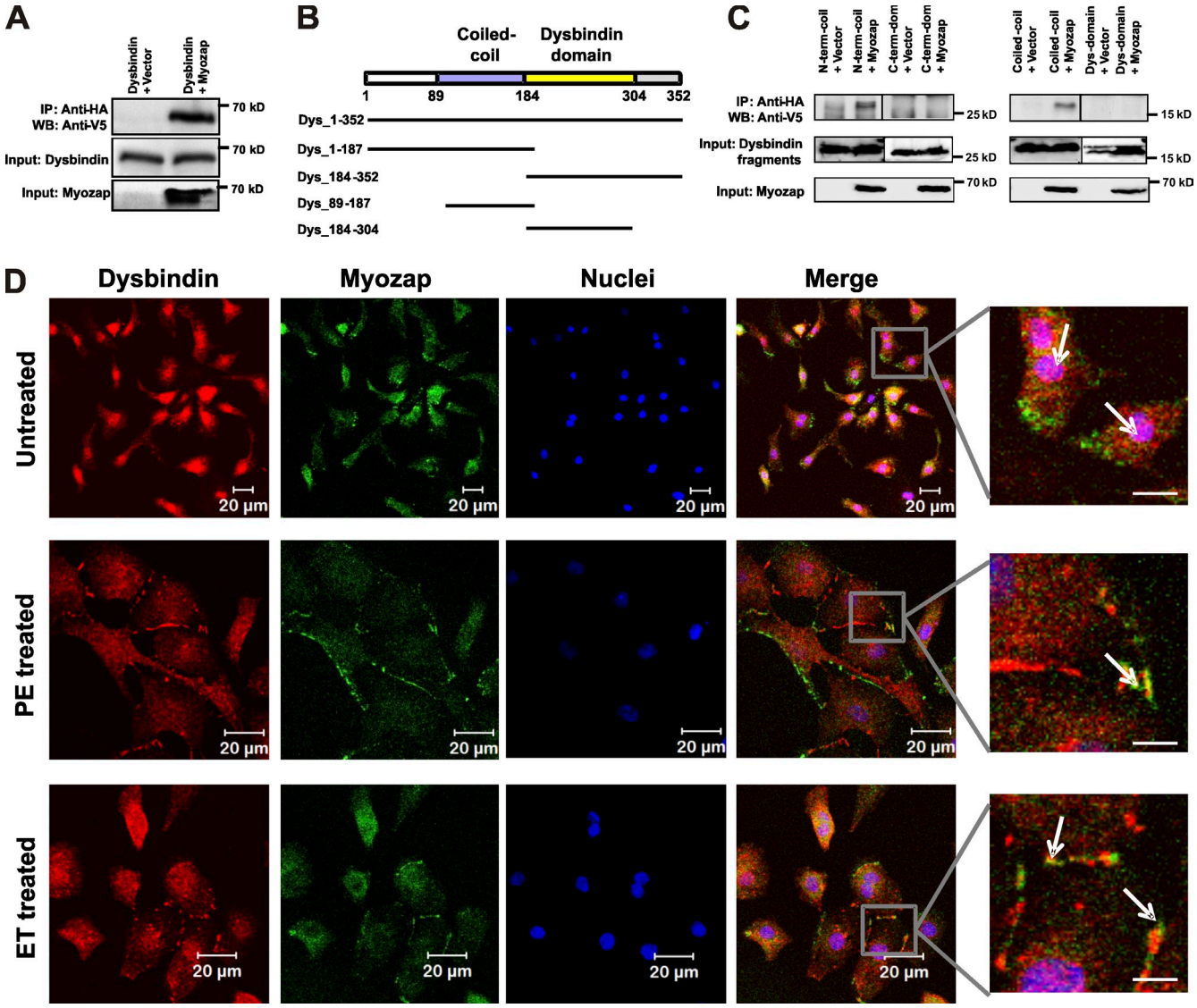

Figure 1. **Dysbindin interacts with Myozap.** (A) Co-IP of Myozap and Dysbindin. HEK293A cells were transfected with plasmids encoding HA-tagged Myozap and V5-tagged Dysbindin. Immunoprecipitation was performed using EZview Red Anti-HA Affinity Gel as described in the Materials and methods. Empty vector expressing HA was used as a negative control. Precipitated proteins were immunoblotted with V5 antiserum. Dysbindin was coprecipitated with Myozap (lane 2), whereas no signal could be seen with empty vector (lane 1), confirming the interaction between Dysbindin–Myozap. (B) Schematic diagram showing different domain fragments constituting Dysbindin used to map the exact domain responsible for interaction with Myozap. (C) Co-IP was performed using four different fragments of Dysbindin as described in A. Black lines indicate that intervening lanes have been spliced out. (D) Coimmunostaining of Dysbindin with Myozap in untreated, 50 µM phenylephrine (PE)-treated, or 1 µM endothelin-1 (ET)–treated NRVCMs. Nuclei were stained with DAPI, and the immunofluorescence images were captured on a confocal microscope (LSM 510). Arrows indicate colocalization of Dysbindin–Myozap. WB, Western blot. Bars: (top inset) 10 µm; (middle and bottom insets) 20 µm.

Dysbindin–RhoA interaction first by co-IP in HEK293A cells using coexpressed HA-tagged and V5-tagged recombinant RhoA and Dysbindin proteins, respectively (Fig. 3 B). Additionally, we could precipitate endogenous RhoA with Dysbindin antibody in proteins isolated from NRVCMs and mouse heart (Fig. 3 C). Furthermore, Dysbindin colocalizes with RhoA in the cytosol and perinuclear region in NRVCMs (Figs. 3 D), suggesting the direct and physiological interaction between Dysbindin and RhoA.

Dysbindin activates SRF signaling via RhoA

To explore a functional role of Dysbindin–RhoA interaction, we repeated the aforementioned SRF-RE reporter luciferase assay of Dysbindin in the absence or presence of RhoA overexpression. As expected, coexpression of Dysbindin and RhoA displayed an additive effect on luciferase activity (Fig. 4 A). Conversely, knockdown of Dysbindin had no inhibitory effect on RhoA-mediated activation on luciferase activity (Fig. 4 B and Fig. S2, E–G), pointing toward Dysbindin being upstream of RhoA in signaling cascade.

RhoA–SRF signaling is essential for regulation of the muscle genes expression. Because we identified RhoA as a novel binding partner of Dysbindin, we hypothesized that Dysbindin induces activation of SRF signaling via RhoA. To test this hypothesis, we again performed an SRF-RE reporter luciferase assay in the presence of commercially available, cell-penetrating

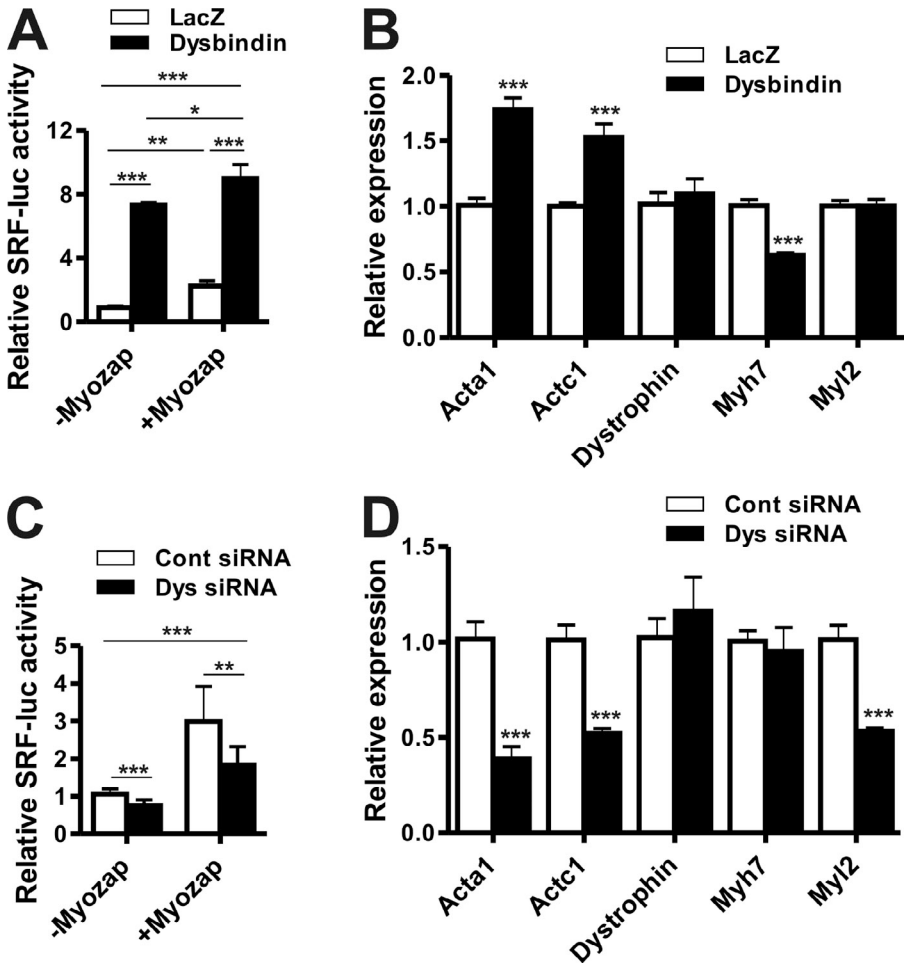

Figure 2. **Overexpression of Dysbindin induces SRF signaling in cardiomyocytes.** (A) Effect of Myozap and Dysbindin (Dys) on luciferase activity determined by SRF-RE firefly luciferase reporter assay in NRVCMs. Adenoviruses expressing Dysbindin (Ad-Dysbindin), Myozap (Ad-Myozap), SRF-RE reporter–based firefly luciferase (Ad-SRF-luc), and Renilla luciferase (Ad-Renilla, control) were used in NRVCMs. Adenovirus expressing β-galactosidase (Ad-LacZ) was used as a control or to maintain the equal quantity of the infected virus. Virus load used was 20 ifu Ad-Dysbindin, 20 ifu Ad-Myozap, 10 ifu Ad-SRF-luciferase, and 10 ifu Ad-Renilla in different combinations as shown in the figure. Data shown are means of three independent experiments performed in quadruplicates. (B) Expression of cardiac-specific SRF targets such as smooth muscle α-actin (*Acta1*), cardiac α-actin (*Actc1*), dystrophin, myosin heavy chain 7 (Myh7), and myosin light chain 2 (Myl2) was determined by qRT-PCR. $n = 6$. (C) siRNA against Dysbindin was used to knock down the endogenous Dysbindin expression in NRVCMs to study the effect on activation of SRF signaling by luciferase assay. Scrambled unrelated siRNA was used as a control (Cont). Data shown are means of three independent experiments performed in quadruplicates. (D) Expression of cardiac-specific SRF-targets same as in Fig. 2 B, determined by qRT-PCR using cDNA prepared from Dysbindin siRNA-transfected NRVCMs. $n = 6$. Statistical significance was determined using two-tailed Student's *t* test or by two-way ANOVA. Error bars show means ± SEM. *, $P < 0.05$; **, $P < 0.01$; ***, $P < 0.001$.

C3 transferase, a RhoA inhibitor. Of note, C3 transferase completely inhibited the Dysbindin-mediated increase in the luciferase activity (Fig. 4 C). Dysbindin overexpression increases the expression of *acta1* and *actc1* as shown in Fig. 2 B. Interestingly though, upon C3 transferase treatment, expression of *acta1* and *actc1* was reduced by 60–70% despite the overexpression of Dysbindin (Fig. 4 D). Besides, purified, recombinant C3 transferase mutant (E174Q), which lacks RhoA inhibitory activity (Fig. 4 E), did not abrogate Dysbindin-mediated activation of SRF signaling (Fig. 4 F), substantiating direct involvement of RhoA activation in the course of Dysbindin effect.

Dysbindin activates ERK1-dependent MAPK pathway

The SRF gene is also a downstream target of MAPK signaling pathways. Therefore, we studied the effect of Dysbindin on the activation of key components, such as ERK1/2, ERK5, and MAPK p38. We overexpressed Dysbindin in NRVCMs, whereas, Ad-LacZ–infected cells were used as a control, and the extracted protein was used for immunoblotting. The only MAPK highly activated by Dysbindin overexpression was ERK1, whereas activation of ERK5 and p38 was largely unaffected (Fig. 5, A–C). In contrast, activation of ERK2 was inhibited significantly, despite unchanged levels of total ERK2 (Fig. 5 A). Surprisingly, although there was no noticeable activation of ERK5, total ERK5 expression was significantly down-regulated in Dysbindin-overexpressing NRVCMs (Fig. 5 B). Recently, it has been reported that overexpression of Dysbindin exerts neurotrophic effect through activation of Akt signaling pathway (Numakawa et al., 2004). However, in cardiomyocytes, we observed no effect on Akt activation by Dysbindin overexpression under our experimental conditions (Fig. 5 D).

Dysbindin induces hypertrophy in cardiomyocytes

Next, we asked whether Dysbindin is differentially regulated in models of hypertrophy and/or cardiomyopathy, such as PE-treated or stretch-induced cardiomyocytes (in vitro), and aortic banded or Calsarcin knockout (KO) or muscle LIM protein KO mice (in vivo). Although there was no substantial effect in vitro (Fig. S3, A and B), expression of Dysbindin was significantly reduced in murine models of hypertrophy and cardiomyopathy (Fig. S3, C–E). Thus, we investigated whether forced expression or down-regulation of Dysbindin modulates cardiomyocyte hypertrophy. NRVCMs were infected with adenovirus encoding Dysbindin (Ad-Dysbindin), and overexpression of Dysbindin-compared with Ad-LacZ–treated control cells was confirmed by immunoblotting (Fig. 6 A). Next, we determined the expression of hypertrophic marker genes, such as *Nppa* and *Nppb*. Of

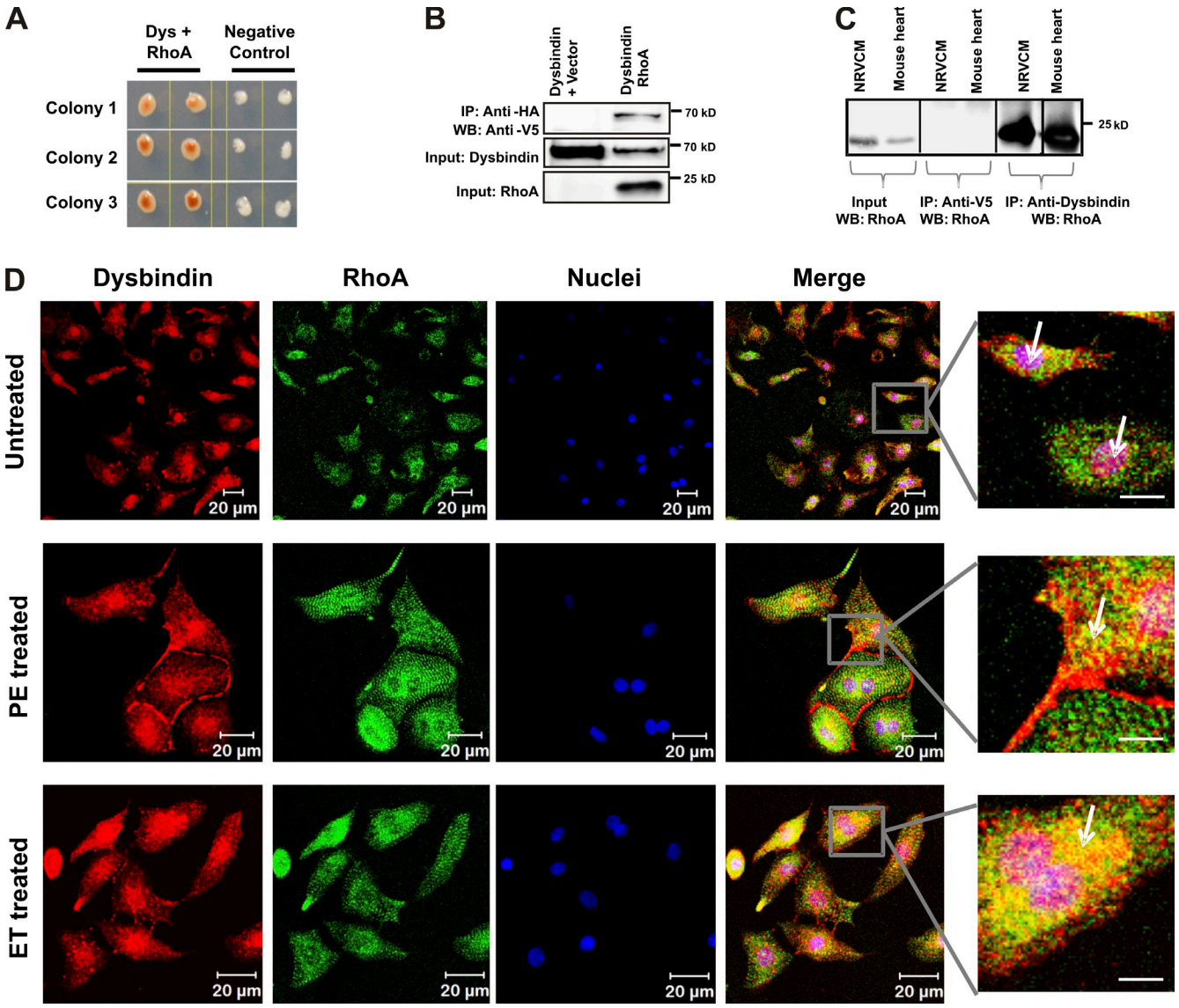

Figure 3. **RhoA is a novel binding partner of Dysbindin.** (A) A representative picture showing the positive interaction between Dysbindin (Dys) and RhoA determined by Y2H assay. Three colonies were spotted in duplicates, and negative control carries empty prey vector. (B) Co-IP of RhoA and Dysbindin. HEK293A cells were transfected with plasmids encoding HA-tagged RhoA and V5-tagged Dysbindin. Immunoprecipitation was performed using EZview Red Anti-HA Affinity Gel following the manufacturer's instructions. Empty vector expressing HA was used as a negative control. (C) Endogenous immunoprecipitation performed with proteins isolated from NRVCMs and mouse heart using V5 antibody (as a control) or with Dysbindin. Immunoblotting was performed with RhoA antibody. Black lines indicate that intervening lanes have been spliced out. (D) Coimmunostaining of Dysbindin with RhoA in untreated, 50 µM phenylephrine (PE)-treated, and 1 µM endothelin-1 (ET)–treated NRVCMs. Nuclei were stained with DAPI, and the immunofluorescence images were captured in a confocal microscope (LSM 510). Arrows indicate colocalization of Dysbindin–RhoA. WB, Western blot. Bars: (top inset) 10 µm; (middle and bottom insets) 20 µm.

note, significant up-regulation of these genes was observed in Ad-Dysbindin–infected cardiomyocytes compared with Ad-LacZ–infected control cells (Fig. 6 B). Additionally, we determined whether overexpression of Dysbindin affects NRVCM cell surface area. PE-treated cells were used as a positive control for cardiomyocyte hypertrophy. Interestingly, we observed a significantly increased cell size of NRVCMs overexpressing Dysbindin (~45–50%, $P < 0.01$), even comparable to the increased cell size induced by PE treatment (~50–55%, $P < 0.01$; Fig. 6, C and D). Strikingly, there was no additive or synergistic effect of PE on Dysbindin-induced hypertrophy (Fig. 6, C and D). Moreover, overexpression of Dysbindin significantly increased both protein/DNA and RNA/DNA ratios, suggesting accelerated protein synthesis (Fig. 6 E). Also, cardiomyocytes overexpressing Dysbindin illustrated well-organized sarcomeric structure compared with control cells, studied by phalloidin staining (Fig. 6 F).

To confirm whether Dysbindin is both necessary and sufficient to induce hypertrophy in NRVCMs, we knocked down its expression using siRNA. Scrambled, unrelated siRNA was used as a control. The knockdown of Dysbindin was confirmed by qRT-PCR and immunoblotting (Fig. 6, G and H). We used varying concentrations of PE (5, 25, and 100 µM) or ET (0.3 and 1 µM) as an inducer of hypertrophic gene program and studied the effect of Dysbindin knockdown. Knockdown of Dysbindin significantly reduced the cell surface area in untreated and 5 µM, but not at 25/100 µM PE-treated NRVCMs (Fig. 6 I and Fig. S3, F–H). This could possibly be because being a potent adrenergic agonist such as PE, administered at high doses, may induce other

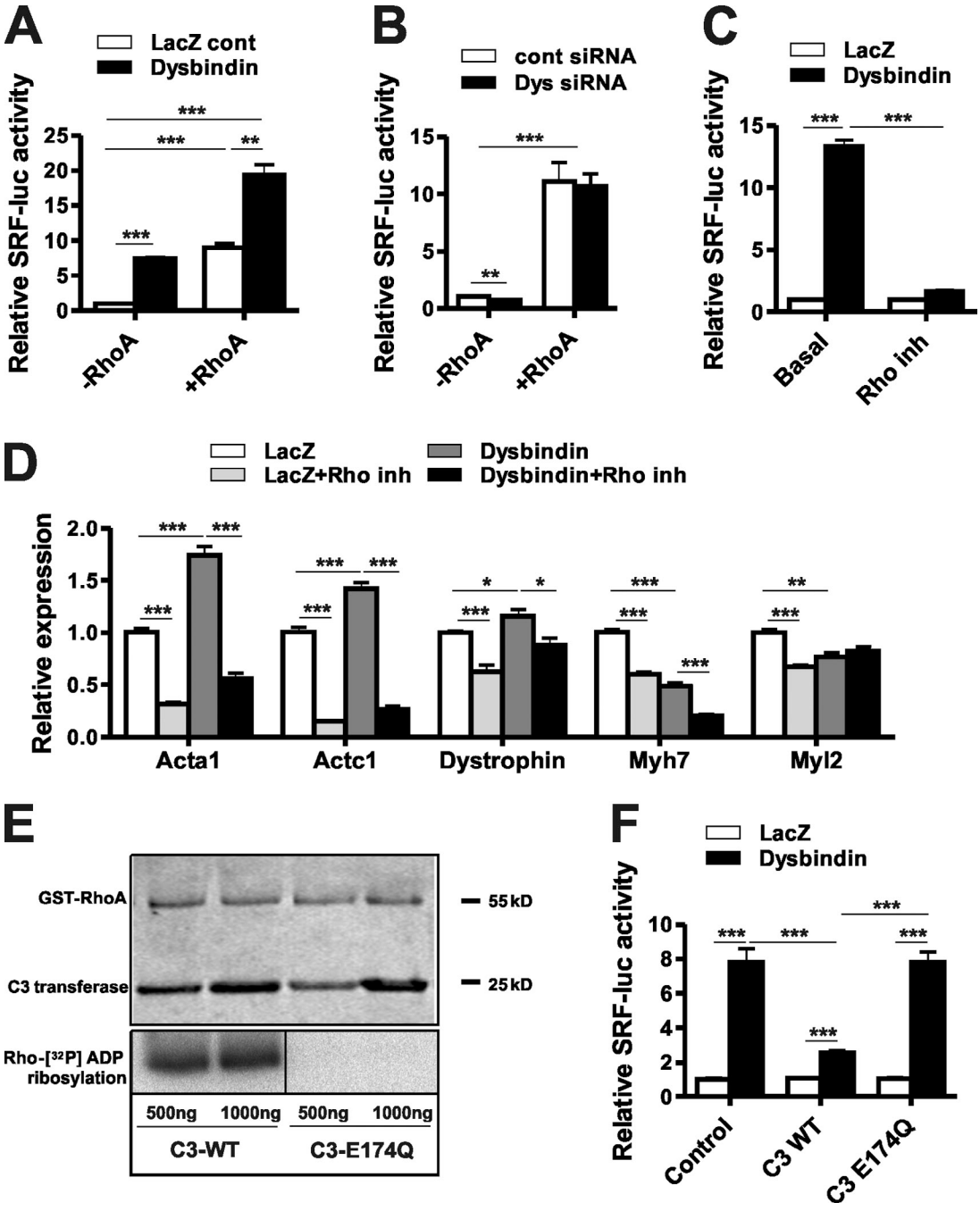

Figure 4. **Dysbindin activates SRF signaling via RhoA.** (A) Effect of RhoA and Dysbindin on luciferase activity determined by SRF-RE firefly luciferase reporter assay in NRVCMs. Adenoviruses expressing Dysbindin (Ad-Dysbindin), RhoA (Ad-RhoA), SRF-RE reporter-based firefly luciferase (Ad-SRF-luc), and Renilla luciferase (Ad-Renilla, control) were used in NRVCMs. Adenovirus expressing β-galactosidase (Ad-LacZ) was used as a control or to maintain the equal quantity of the infected virus. Infectious units of viruses used were 20 ifu Ad-Dysbindin, 20 ifu Ad-RhoA, 10 ifu Ad-SRF-luciferase, and 10 ifu Ad-Renilla in different combinations as shown in the figure. Data shown are means of two independent experiments performed in hexaplicates. (B) siRNA against Dysbindin (Dys) was used to knockdown endogenous Dysbindin expression in NRVCMs to study the activation of SRF signaling by luciferase assay. Scrambled unrelated siRNA was used as a control. Data shown are means of two independent experiments performed in hexaplicates. cont, control. (C) Effect of Rho inhibitor C3 transferase (commercially available) on luciferase activity. $n = 6$. (D) Similar conditions as used for C3 transferase treatment in Fig. 4 C were used to study the expression of SRF gene targets such as smooth muscle α-actin (*Acta1*), cardiac α-actin (*Actc1*), dystrophin, myosin heavy chain 7 (Myh7), and myosin light chain 2 (Myl2) by qRT-PCR. $n = 6$. inh, inhibitor. (E) 2 µM GST-RhoA was incubated with the wild-type C3 transferase or mutant protein at various concentrations and 1 µCi [^{32}P]NAD$^+$ in 20 µl of reaction buffer at 37°C for 20 min. The reaction was terminated by addition of Laemmli sample buffer and then incubated at 95°C for 10 min. Samples were resolved by SDS-PAGE on 15% gels, and the ADP-ribosylated RhoA was analyzed by phosphorimaging (no molecular weight marker was run along in the bottom blot). The black line indicates that intervening lanes have been spliced out. WT, wild type. (F) C3 transferase and its point mutant (E174Q) were purified as recombinant GST fusion proteins in *E. coli* TG1 cells and used for luciferase assays as described in Fig. 4 A. Data shown are means of two experiments performed in triplicates. Statistical significance was determined using two-tailed Student's *t* test or two-way ANOVA. Error bars show means ± SEM. *, $P < 0.05$; **, $P < 0.01$; ***, $P < 0.001$.

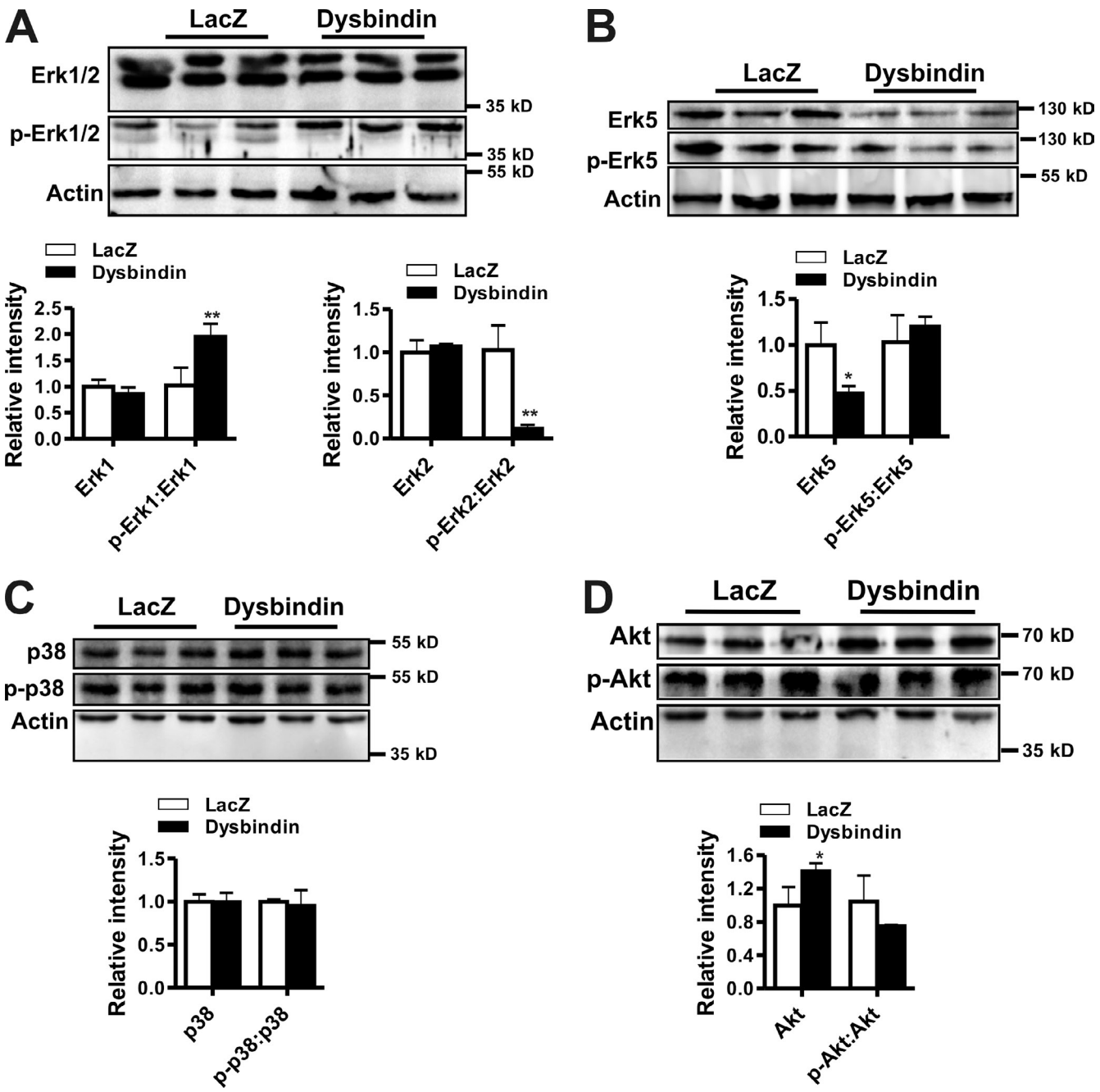

Figure 5. **Dysbindin activates the ERK1-dependent MAPK pathway.** Cultured NRVCMs were infected with adenovirus expressing Dysbindin (Ad-Dysbindin; 20 ifu) in serum-free media for 72 h and used for protein extraction. Adenovirus expressing β-galactosidase (Ad-LacZ) is used as a control. (A–D) Immunoblotting was performed against ERK1/2 and phospho-ERK1/2 (p-ERK1/2; A), ERK5 and phosphor-ERK5 (B), MAPK p38 and phosphor-p38 (C), and Akt and phosphor-Akt (D). Densitometric analysis was performed using α-actin as a loading control. Data shown are representative of two independent experiments performed in duplicates or triplicates. Statistical significance was determined using two-tailed Student's *t* test. Error bars show means ± SEM. *, $P < 0.05$; **, $P < 0.01$.

hypertrophic signaling pathways, which cannot sufficiently be inhibited by dysbindin knockdown alone. Of note, dysbindin knockdown significantly subdued the prohypertrophic effect of ET at two dosages (Fig. 6 J).

RhoA and ERK1 inhibition abrogates the prohypertrophic effects of Dysbindin

To further confirm the direct or indirect involvement of RhoA and ERK1 in the Dysbindin-mediated activation of hypertrophy, we studied the effect of C3 transferase and a MEK1 inhibitor (PD98059) on the expression of hypertrophic markers as well as cell surface area. C3 transferase treatment resulted in reduced expression of both natriuretic peptides (*Nppa* and *Nppb*; Fig. 7 A). Moreover, C3 transferase clearly exerted phenotypic effects on cardiomyocytes. Control cells as well as Dysbindin-overexpressing NRVCMs were reduced in size and showed an impaired actin cytoskeleton upon C3 transferase treatment as shown in Fig. 7 (B and C; see also Fig. S4 A). Likewise,

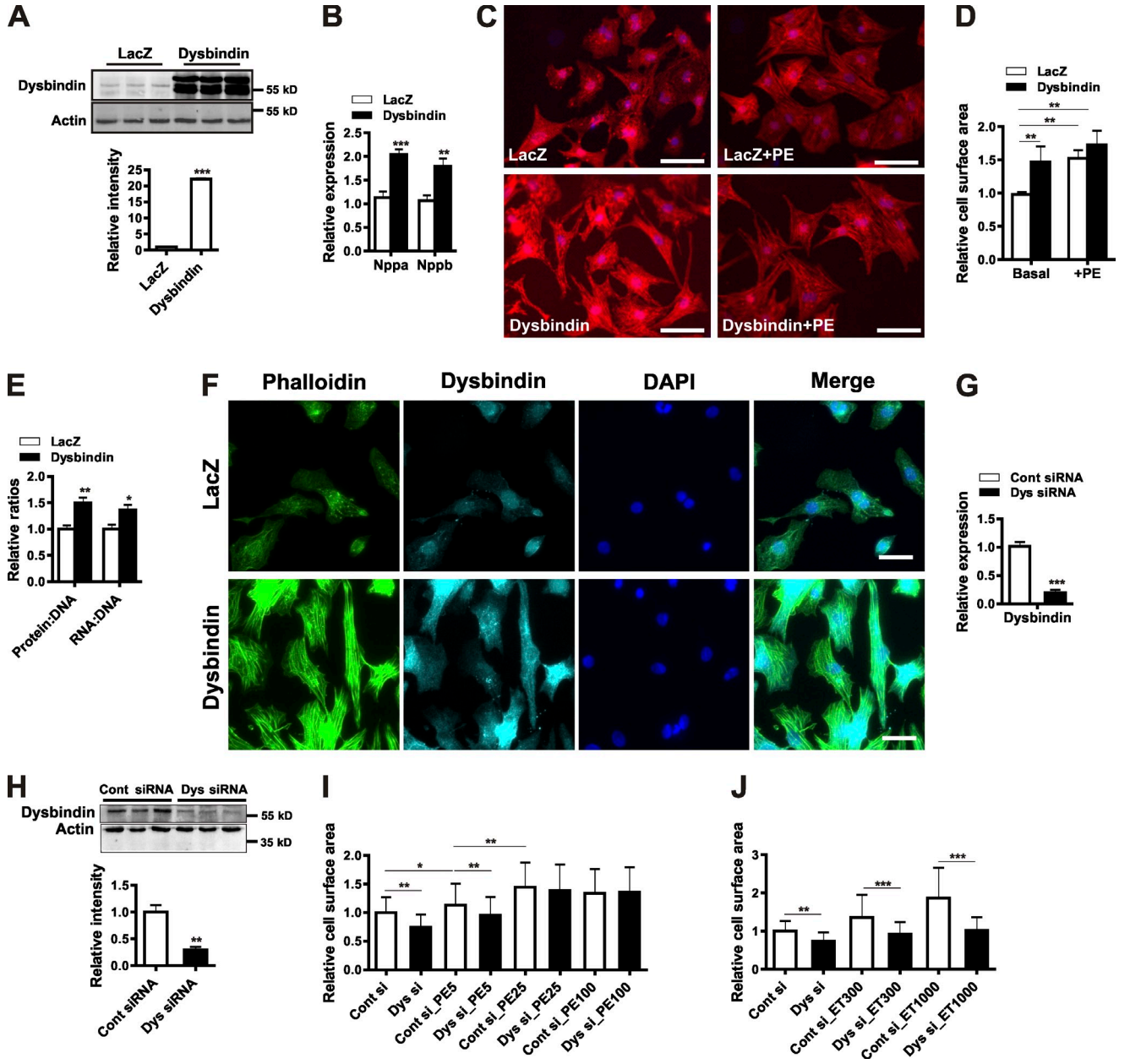

Figure 6. **Dysbindin induces hypertrophy in cardiomyocytes.** (A) Overexpression of Dysbindin was confirmed by immunoblotting in NRVCMs infected with Adenovirus expressing Dysbindin (Ad-Dysbindin; 20 ifu) in serum-free media for 72 h. Adenovirus expressing β-galactosidase (Ad-LacZ) was used as a control. (B) Expression of hypertrophic gene markers *Nppa* and *Nppb* was determined using qRT-PCR in Dysbindin-overexpressing NRVCMs. Data shown are means of two independent experiments in hexaplicate. (C) Representative images showing the phenotypic effect of Dysbindin overexpression. NRVCMs were cultured on coverslips in triplicates, infected with Ad-Dysbindin/Ad-LacZ for 72 h, and immunostained with α-actinin. Nuclei were stained with DAPI. (D) Cell size measurements: Cell surface area was measured from randomly selected 300 or more cells from three different coverslips using ImageJ software. Ad-LacZ–infected NRVCMs treated with 50 µM PE were used as a positive control. (E) DNA, protein, and RNA were isolated from LacZ (as a control) or Dysbindin-overexpressing NRVCMs, and protein/DNA and RNA/DNA ratios were determined. $n = 6$. (F) Representative images showing phenotypic effect of Dysbindin on actin cytoskeleton by FITC-labeled Phalloidin, costained with Dysbindin. Nuclei were stained with DAPI. (G and H) Endogenous expression of Dysbindin (Dys) was knocked down using siRNA. Down-regulation of Dysbindin expression was confirmed in Dysbindin siRNA–transfected as compared with the control (Cont) siRNA–transfected NRVCMs by qRT-PCR (G) and immunoblotting (H). Data shown are means of three independent experiments in triplicate. (I and J) NRVCMs were either untreated as control or treated with 5, 25, or 100 µM PE (I) or 0.3 or 1 µM ET (J) and processed as in Fig. 6 C. Images were captured on Keyence microscope, and cell surface area was measured using MacroCellCount analyzer as detailed in the Materials and methods. Statistical significance was determined using two-tailed Student's *t* test or by one/two-way ANOVA. Error bars show means ± SEM. *, $P < 0.05$; **, $P < 0.01$; ***, $P < 0.001$. Bars, 50 µm.

use of the MEK1 inhibitor resulted in substantial reduction in the expression of *Nppa* and *Nppb* in Ad-LacZ–infected control cells (Fig. 7 D). A similar effect, i.e., down-regulation of *Nppa* and *Nppb* was observed in Ad-Dysbindin–infected cells (Fig. 7 D) in the presence of MEK1 inhibitor. Furthermore, the cell surface area of MEK1 inhibitor–treated cells was significantly reduced compared with the untreated cells, though the effect was moderate in Dysbindin-expressing cells compared with the control cells (Fig. 7, E and F). In the same lines, NFAT (nuclear factor of activated T cells)/Calcineurin is one of the

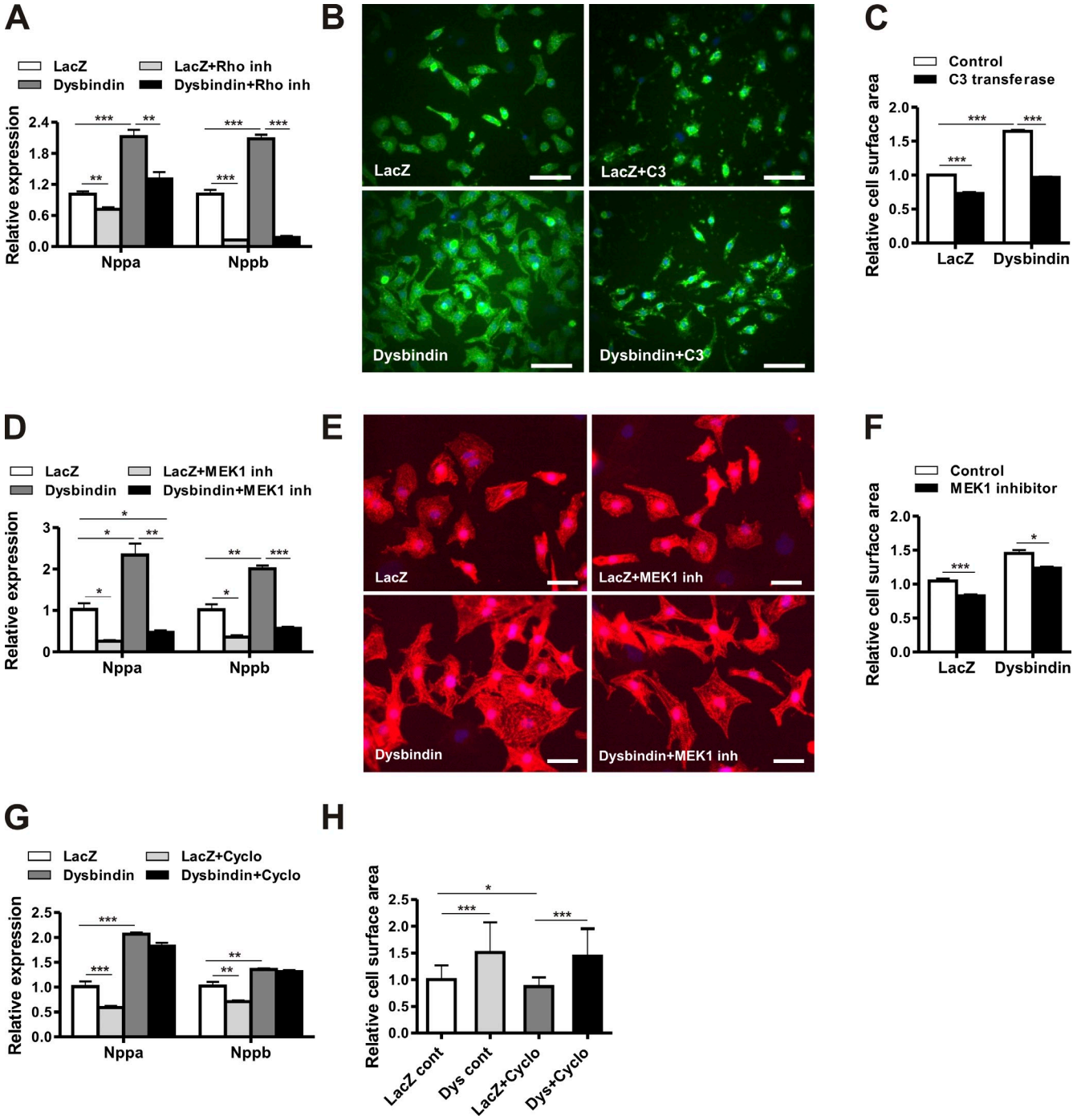

Figure 7. **RhoA and ERK1 inhibition abrogates the prohypertrophic effects of Dysbindin.** (A) Expression of hypertrophic gene markers *Nppa* and *Nppb* was determined by qRT-PCR in Dysbindin-overexpressing NRVCMs in the absence or presence of C3 transferase, a RhoA inhibitor. LacZ-overexpressing cells were used as a control group. $n = 6$. (B) Representative images showing the phenotypic effect of C3 transferase. NRVCMs were cultured on coverslips in triplicates, infected with Adenovirus expressing Dysbindin/LacZ for 72 h, and immunostained with α-actinin. Nuclei were stained with DAPI. Cells were treated with C3 transferase 12 h before immunostaining. (C) Cell surface area of C3 transferase treatment datasets was measured from randomly selected 300 or more cells from three different coverslips using ImageJ software. (D) Expression of *Nppa* and *Nppb* was determined in Ad-LacZ– or Ad-Dysbindin–infected NRVCMs in the absence or presence of MEK1 inhibitor by qRT-PCR. $n = 6$. (E) Representative images showing the phenotypic effect of MEK1 inhibitor (inh). (F) Cell surface area of MEK1 inhibitor treatment datasets was measured from randomly selected 300 or more cells from three different coverslips using ImageJ software. (G) Expression of *Nppa* and *Nppb* was determined in Ad-LacZ– or Ad-Dysbindin–infected NRVCMs in the absence or presence of Cyclosporin A, a Calcineurin inhibitor, by qRT-PCR. $n = 6$. (H) NRVCMs overexpressing Dysbindin (Dys; or LacZ as control [cont]) were either untreated or treated with Cyclosporine A (Cyclo) and processed as in Fig. 7 B. Immunoimages were captured on Keyence microscope, and cell surface area was measured using MacroCellCount analyzer as detailed in the Materials and methods. Statistical significance was determined using two-tailed Student's *t* test or by one/two-way ANOVA. Error bars show means ± SEM. *, $P < 0.05$; **, $P < 0.01$; ***, $P < 0.001$. Bars, 50 μm.

major pathways associated with cardiac hypertrophy. Nevertheless, inhibition of this pathway by cyclosporin A did not significantly reduce the prohypertrophic effects of Dysbindin (Fig. 7, G and H).

Discussion

Numerous studies have independently associated Dysbindin with the progression of schizophrenia (Schwab et al., 2003; Talbot et al., 2004, 2011; Bray et al., 2005; Allen et al., 2008). Though it was reported to be ubiquitously expressed in various tissues, Dysbindin research is so far focused mostly on its role and function in the brain. In our current study, we show a novel role for this protein in cardiomyocyte signaling and its involvement in SRF- and ERK1-dependent hypertrophy. This study further highlights the identification of Dysbindin as a novel interaction partner of small GTPase RhoA and the junctional protein Myozap. Specifically, we show that Dysbindin induces RhoA-dependent activation of SRF signaling, both alone and in tandem with Myozap. Additionally, adenovirus-mediated overexpression of Dysbindin strongly induces hypertrophy in NRVCMs in concert with the activation of RhoA–SRF and ERK1 signaling pathways.

Recently, our group has identified and characterized the novel cardiac protein Myozap. In vitro data suggested the involvement of Myozap in the induction of Rho-dependent SRF signaling via binding with MRIP (Seeger et al., 2010). Apart from MRIP, Myozap was shown to interact and/or colocalize with β-Catenin and N-Cadherin as well as Plakophilin-2 at the ID of cardiomyocytes and directly binds to ID components, such as Desmoplakin and ZO-1 (Zonula Occludens-1; Seeger et al., 2010). Interestingly, Dysbindin was first described as a binding partner of Dystrobrevins, which are known to be localized to the cell membrane of muscle as well as nonmuscle cells (Holzfeind et al., 1999; Benson et al., 2004; Lien et al., 2004; Rees et al., 2007). Dysbindin fascinated neurobiologists when Straub et al. (2002) reported an association of genetic variants in the Dysbindin gene *DTNBP1*, located on chromosome 6p22.3, with an increased risk of schizophrenia. Thereafter, many independent groups have correlated several mutations and/or expression levels of Dysbindin with the onset of schizophrenia in humans (Schwab et al., 2003; Talbot et al., 2004, 2011; Bray et al., 2005; Allen et al., 2008; Strohmaier et al., 2010). Also, Dysbindin is one of the major components of BLOC-1 (biogenesis of lysosome-related organelles complex 1) causing HPS-7 (Hermansky–Pudlak syndrome type 7; Li et al., 2003). Here, in a Y2H screen aimed to determine the cardiac-specific binding partners of Myozap, we identified Dysbindin as one of its interaction partners. The binding region of Dysbindin was mapped to its N-terminal coiled-coil domain. Notably, Myozap also consists of a long coiled-coil domain, and thus, it is likely that coiled-coil region from both the proteins could mediate this interaction. Moreover, the coiled-coil domain of Dysbindin was previously shown to interact with Dystrobrevins and Myospryn, suggesting its essential role in structural and/or functional interactions with other proteins (Benson et al., 2001, 2004). Additionally, immunofluorescence experiments revealed colocalization of Dysbindin and Myozap at the membrane, upon induction of hypertrophy, further confirming their potential cellular interaction. Nevertheless, Dysbindin was predominantly localized to the nucleus in NRVCMs and ARVCMs, suggesting dynamic regulation of its localization depending on cellular physiological state. Nuclear localization in cardiomyocytes suggests that Dysbindin might also have a role in gene transcription of cardiomyocytes, which remains to be explored.

SRF is a ubiquitously expressed, multifunctional transcription factor, which regulates the expression of various muscle genes by binding to its specific promoter sequence known as CArG box (Shore and Sharrocks, 1995; Miano, 2010; Kuwahara and Nakao, 2011). SRF is known to act through at least two known pathways. First, it interacts with ternary complex factors, which are regulated by MAPK signaling involving MEK1 and ERK1. The second regulatory pathway involves a group of SRF coactivators called myocardin-related transcription factors, which are controlled by Rho family GTPases. Myocardin-related transcription factors mediate prohypertrophic signaling by linking Rho-actin dynamics to cardiac gene transcription (Kuwahara and Nakao, 2011). Our previous work illustrated that Myozap induces Rho-dependent activation of SRF signaling (Seeger et al., 2010). In the present study, adenovirus-mediated overexpression of Dysbindin dramatically activated SRF-dependent reporter genes. Of note, Dysbindin-induced activation of luciferase activity was three- to fourfold higher than that of Myozap alone. Nevertheless, Dysbindin exhibited an additive activation of SRF signaling in the presence of Myozap. Likewise, Dysbindin overexpression led to strong upregulation of *acta1* and *actc1*, major components of actin cytoskeleton, and fetal cardiac genes *Nppa* and *Nppb*, which are also known SRF targets. These changes were accompanied by an increased cell size, i.e., cardiomyocyte hypertrophy. To the contrary, knockdown of Dysbindin reduced the activation of SRF signaling and cellular hypertrophy, suggesting its essential involvement in this mechanistic pathway.

An interesting finding of our study is the identification of RhoA as a novel binding partner of Dysbindin validated by several measures, such as the Y2H assay, immunoprecipitation, and immunostaining. Moreover, use of C3 transferase (which selectively inhibits RhoA/B/C and not Cdc42/Rac1) and its E174Q point mutant (which lacks RhoA inhibitory effect) enabled us to determine the direct involvement of Dysbindin in RhoA-mediated induction of SRF signaling and hypertrophy in NRVCMs. The Dysbindin–RhoA interaction thus provides a plausible underlying mechanism for the observed effects on SRF. Collectively, these data make stand out robust RhoA-dependent activation of SRF signaling as well as cardiomyocyte hypertrophy.

Dysbindin overexpression reportedly activates Akt signaling in cultured neurons, thereby protecting cortical neurons against neuronal death as a result of serum deprivation (Numakawa et al., 2004). Nonetheless, in cardiomyocytes, we did not observe activation of Akt signaling pathway by Dysbindin overexpression, pertaining to its distinct mechanistic effects in different cell types, here for instance in the brain and the heart. Instead, overexpression of Dysbindin led to significant activation of ERK1 MAPK that could supplement the induction of SRF

signaling and hypertrophy in NRVCMs. This fact was further validated by inhibiting the basal activation of ERK1/2 by a MEK1 inhibitor in the absence or presence of Dysbindin. The MEK1 inhibitor used in this study (PD98059) selectively inhibits the activation of MEK1, which in turn blocks the activation of ERK1/2. These experiments demonstrated that the hypertrophic effect of Dysbindin was modulated by MEK1 inhibitor but to a lesser extent than by the RhoA inhibitor C3 transferase. These observations suggest mutual or cooperative involvement of RhoA–SRF and MEK1–ERK1 signaling pathways in Dysbindin-driven hypertrophy. Altogether, our data specify that Dysbindin-mediated induction of SRF signaling and hypertrophy likely integrates different intracellular signaling pathways (Fig. 8).

MRIP, a Rho inhibitor, was earlier reported by our group as a binding partner of Myozap. Here, we show that Dysbindin binds and interacts with Myozap, whereas knockdown of Dysbindin by siRNA inhibited Myozap-mediated activation of SRF signaling. Therefore, we believe that binding of Dysbindin to Myozap might suppress the Myozap–MRIP interaction, accelerating the activation of SRF signaling and vice versa. Moreover, the positive interaction between Dysbindin and RhoA may also antagonize the inhibitory effect of MRIP on SRF signaling (Fig. 8). These observations thus indicate a complex regulation of Dysbindin–Myozap-mediated SRF signaling via MRIP and RhoA (Fig. 8).

In summary, our data provide the first line of evidence for a role of Dysbindin in cardiomyocyte physiology and pathophysiology beyond a mere role in neurons. Dysbindin plays a distinct role in cardiac signaling pathways, in particular RhoA–SRF-dependent transcription. On broader terms, further dissection of the role of Dysbindin in cardiomyocytes should also be useful in understanding more about its function in other tissues, including skeletal muscle and brain.

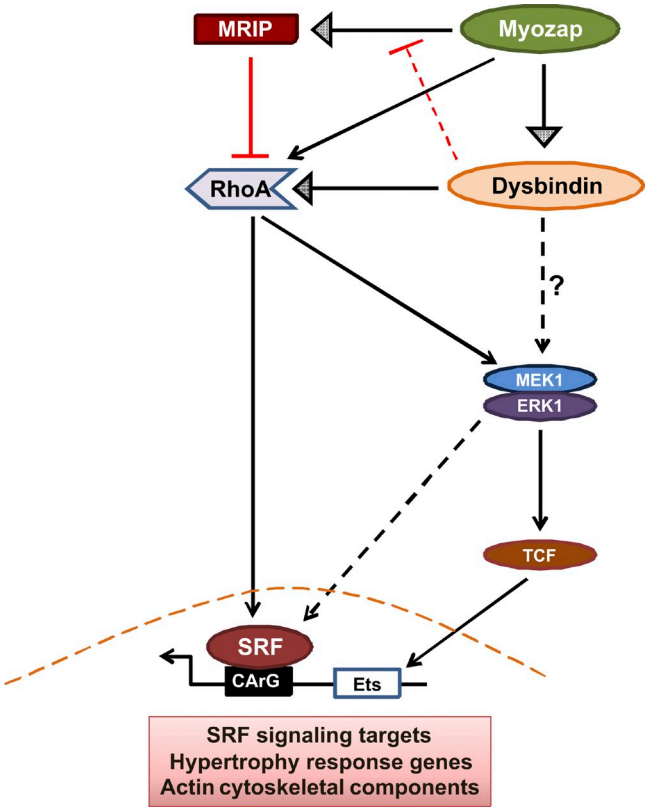

Figure 8. **Model figure for Dysbindin-SRF signaling.** Dysbindin exhibits two different roles to activate SRF signaling. First, Dysbindin along with Myozap and RhoA itself activates RhoA-dependent SRF signaling, which in turn induce the expression of actin cytoskeleton and hypertrophy response genes. Second, Dysbindin moderately activates interdependent MEK1–ERK1 signaling pathways. Myozap on the other hand can activate RhoA–SRF signaling, which gets inhibited by its interaction with Myosin phosphatase Rho-interacting protein (MRIP). Dysbindin–Myozap interaction possibly hinders Myozap–MRIP interaction, positively and cooperatively activating RhoA–SRF signaling in cardiomyocytes. Ets, E26 transformation specific; TCF, ternary complex factor.

Materials and methods

Cloning of full length and partial fragments of *Dysbindin*

Full-length and partial fragments (as shown in Fig. 1 C) of mouse Dysbindin were cloned from mouse heart cDNA by using primers listed in Table S1 for a first step PCR and attB forward, 5′-GGGGACAAGTTTGTACAAAAAAGCTGGCACC-3′, and attB reverse, 5′-GGGGACCACTTTGTACAAGAAAGCTGGGTCGCC-3′, for a second step PCR. The PCR product was recombined into the pDonR221 plasmid (Life Technologies) using the Gateway technology and was subsequently recombined into expression plasmid pDest40 to obtain V5-tagged expression constructs.

Cloning of SRF-RE reporter firefly luciferase and Renilla luciferase

Template plasmids used for cloning SRF-RE reporter firefly luciferase and Renilla luciferase were purchased from Promega (plasmid pGL4.34[*luc2P*/SRF-RE/Hygro] and pGL4.74[*hRluc*/TK], respectively). Forward primers (including attB sites needed for recombination) used for firefly and Renilla luciferase were 4.34_attB forward, 5′-GGGGACAAGTTTGTACAAAAAAGCTGGCTAGTATGTCCATATTAGGACATCTACC-3′, and 4.74_attB forward, 5′-GGGGACAAGTTTGTACAAAAAAGCTGGCTAAATGAGTCTTCGGACCTCG-3′, respectively, whereas the reverse primer was common for both: pGL4_attBRpA, 5′-GGGGACCACTTTGTACAAGAAAGCTGGGTTTTACCACATTTGTAGAGGTTTTACTTG-3′. The PCR product was recombined into the pDonR221 plasmid (Life Technologies) using the Gateway technology and was subsequently used to generate respective adenoviruses as described in the following paragraph.

Generation of recombinant adenoviruses and recombinant protein expression plasmids

An adenovirus encoding the full-length mouse Dysbindin, Myozap, or RhoA cDNA and other necessary constructs (SRF-RE–luciferase, Renilla luciferase, etc.) were generated using the ViraPower Adenoviral kit (Life Technologies) according to the manufacturer's instructions. In brief, a cDNA that had been previously cloned into the pDonR221 vector was shuttled into the pAd/cytomegalovirus/V5-DEST Gateway vector. PacI restriction enzyme digested pAd/cytomegalovirus/V5-DEST constructs were transfected into HEK293A cells to produce respective protein-expressing adenoviruses. Titration of the virus was performed by staining infected HEK293A cells with fluorescent anti-Hexon antibody. A β-galactosidase-V5–encoding adenovirus (Ad-LacZ; Life Technologies) served as a control. Similarly, for the generation of expression plasmids, respective genes cloned into pDonR221 vector were shuttled into pDest40, a Gateway expression vector for mammalian cells.

Antibodies used for immunofluorescence/immunoblotting

Antibodies were as follows: α-actin, goat polyclonal (1:3,000; Santa Cruz Biotechnology, Inc.); α-actinin, mouse monoclonal (1:200; Sigma-Aldrich); Akt, rabbit polyclonal (1:1,000; Cell Signaling Technology); p-Akt, mouse monoclonal (1:1,000; Cell Signaling Technology); Dysbindin, rabbit polyclonal (1:500; Sigma-Aldrich); ERK1/2, mouse monoclonal (1:2,000; Cell Signaling Technology); p-ERK1/2, rabbit monoclonal (1:1,000; Cell Signaling Technology); ERK5, rabbit polyclonal (1:1,000; Cell Signaling Technology); p-ERK5, rabbit polyclonal (1:1,000; Cell Signaling Technology); MAPK p38, rabbit polyclonal (1:1,000; Cell Signaling Technology); MAPK p-p38, mouse monoclonal (1:2,000; Cell Signaling Technology); Myozap, mouse monoclonal (1:50; Progen); and anti-V5, rabbit polyclonal (1:2,000; Sigma-Aldrich).

Isolation of NRVCMs and ARVCMs

NRVCMs or ARVCMs were prepared as previously described (Boerries et al., 2007; Frank et al., 2010). In brief, for isolation of NRVCMs, left

ventricles from 1–2-d-old Wistar rats (Charles River) were harvested and chopped in ADS buffer containing 120 mmol/liter NaCl, 20 mmol/liter Hepes, 8 mmol/liter NaH_2PO_4, 6 mmol/liter glucose, 5 mmol/liter KCl, and 0.8 mmol/liter $MgSO_4$, pH 7.4. Around five to six enzymatic digestion steps were performed with 0.6 mg/ml pancreatin (Sigma-Aldrich) at 37°C and 0.5 mg/ml collagenase type II (Worthington Biochemical Corporation) in sterile ADS buffer. Cell suspension was passed through a cell strainer followed by the addition of newborn calf serum to stop enzymatic digestion. Cardiomyocytes were separated from fibroblasts using a Percoll (GE Healthcare) gradient centrifugation step and cultured in DMEM containing 10% FCS, penicillin/streptomycin, and L-glutamine (PAA Laboratories).

ARVCMs were isolated from male Wistar rats (200–280 g) anaesthetized by intraperitoneal injection of 10 ml Trapanal (0.5 g). Hearts were quickly excised; aorta was cannulated and perfused with the EDTA medium for 5 min at 37°C, at a constant flow rate of 12 ml/min. The heart was retroperfused with collagenase/EDTA medium (60 mg Collagenase and 293 U/ml in 20-ml EDTA-supplemented medium) at 37°C for 30–45 min and cut into small pieces. Minced tissue in the EDTA medium was filtered through a 200-µm nylon filter. Cardiomyocytes were then subjected to increasing Ca^{2+} concentration and centrifugation to obtain calcium stable cardiomyocytes. Supernatant was aspirated, and the cardiomyocyte pellet was resuspended in 20 ml M199 medium and counted with Neubauer chamber.

Co-IP in HEK293A cells

HEK293A cells were maintained in DMEM containing 10% FBS, 2 mM L-glutamine, and penicillin/streptomycin. 2.5×10^6 HEK293A cells were cotransfected with 6 µg each of expression plasmids coding for HA-tagged Myozap (or HA-tagged RhoA) and V5-tagged Dysbindin using Lipofectamine 2000 (Life Technologies). For mapping the exact domain of Dysbindin interacting with Myozap, several fragments were cloned with C-terminal V5 tag and used for co-IP with HA-tagged Myozap. Empty vector pCGN-expressing HA-tag was used as a negative control for all the co-IP experiments. 48 h after transfection, cells were washed with PBS, pelleted, and resuspended in buffer A (50 mM Tris, 150 mM NaCl, 1 mM EDTA, and 5% glycerol) supplemented with protease inhibitor cocktail (Complete; Roche). Cells were lysed by freeze–thaw (twice), and debris was removed by centrifugation. Supernatant-containing protein was used for the immunoprecipitation using anti-HA affinity gel (EZview Red; Sigma-Aldrich) following the manufacturer's protocol. In brief, 1 mg protein in a total volume of 1 ml was applied to 30 µl of equilibrated beads, and HA-tagged proteins were allowed to bind to anti-HA antibody on the beads for ∼4 h at 4°C. Protein lysate was removed carefully after centrifugation at 8,200 *g*, and beads were washed for four to five times with lysis buffer. Precipitated proteins from the beads were eluted with 50 µl Laemmli sample buffer, 10–15 µl of which was subjected to SDS-PAGE followed by transfer to nitrocellulose or polyvinylidene fluoride (PVDF) membranes and immunoblotted using monoclonal anti-V5 antibody (Sigma-Aldrich). All co-IP experiments were performed twice.

Immunoprecipitation of endogenous proteins

Mouse left ventricles were homogenized with a tissue separator (IKA Ultra-Turrax; Sigma-Aldrich), whereas NRVCMs were lysed by two to three freeze–thaw cycles in buffer A. Approximately 4 µg anti-Dysbindin antibody (rabbit polyclonal; Santa Cruz Biotechnology, Inc.), anti-RhoA antibody (mouse monoclonal; Santa Cruz Biotechnology, Inc.), or anti-Myozap antibody (Progen) was allowed to interact with 1 mg protein in a total volume of 1 ml for 4 h at 4°C. Then, 50 µl of equilibrated Dynabeads Sepharose G (Life Technologies) was added, and IgG-bound proteins were allowed to bind to the beads overnight at 4°C. Protein lysate was removed carefully, and beads were washed for four to five times with lysis buffer. Precipitated proteins from the beads were eluted with 50 µl Laemmli buffer, 10–15 µl of which was subjected to SDS-PAGE followed by transfer to nitrocellulose or PVDF membranes and immunoblotted using the monoclonal anti-V5 antibody. All co-IP experiments were performed twice or more.

Immunofluorescence microscopy

Subcellular localization of Dysbindin, its colocalization with Myozap, and cell size measurement were studied in NRVCMs and ARVCMs by immunofluorescence microscopy. NRVCMs and ARVCMs as prepared in Isolation of NRVCMs and ARVCMs were seeded in a 12-well plate on collagen- or laminin-coated coverslips, respectively. ARVMs and NRVCMs were fixed with 4% paraformaldehyde for 10 min, permeabilized, and blocked with 0.1% Triton X-100 in 2.5% BSA for 1 h at room temperature. Cells were then incubated for 1 h with primary antibodies using the following dilutions: monoclonal mouse anti-Myozap (undiluted; Progen), monoclonal mouse anti–α-actinin (1:200; Sigma-Aldrich), monoclonal mouse anti-RhoA (1:200; Santa Cruz Biotechnology, Inc.), and monoclonal rabbit anti-Dysbindin (1:50; Sigma-Aldrich). Respective secondary antibodies conjugated to either FITC or Cy3 (Dianova) were incubated for 1 h at a dilution of 1:200. Vectashield medium with DAPI (Vector Laboratories) or Fluoromount (Biozol) was used for mounting. Fluorescence micrographs for colocalization experiments were taken with a confocal microscope (using Plan Neofluar 40× oil [immersion oil] or 20× objectives with 1.3 or 0.5 NA, respectively; LSM 510 UV; Carl Zeiss). Images were acquired using LSM 510 version 3.2 software and built-in photomultiplier tube camera at 20°C. Images were processed and analyzed by LSM Image Browser 4.2. Fluorescence micrographs for cell size area were captured either on Axiophot 2 microscope (Plan-Neofluar 20× objective NA 0.5; Carl Zeiss) using a color camera (AxioCam) and AxioVision version 4.8 software (Carl Zeiss) at room temperature) or BZ-9000-E HS all-in-one fluorescence microscope (Plan Apochromat 20× objective, NA 0.75; Keyence) using a built-in camera and BZ-II viewer at 20°C. Images were processed and analyzed by BZ-II Analyzer (Keyence) as detailed in the next paragraph). Fluorochromes used for these analyses were Alexa Fluor 647, Cy3, DAPI, and/or FITC.

Cell surface area measurement using BZ-9000 microscope

Immunofluorescence pictures were taken using the BZ-9000 microscope. For each coverslip with fluorescence-stained cells, 5 × 5 × 5 (xyz) pictures were taken in 20× magnification (objective: CFI Plan Apochromat λ 20×; Nikon) in the merge and z-stack mode with a 30% overlap between neighboring pictures and a z pitch of 3.0 µm (BZ-II Viewer 2.1). Images were further processed and analyzed using the BZ-II Analyzer (version 2.1). Picture series were merged, and a full-focus calculation was performed automatically by the BZ-II Analyzer software. The cell size was measured using the HybridCellCount software module (Keyence) with the fluorescence intensity single-extraction mode. First, fluorescence intensity thresholds were set for a reference picture. Thereafter, α-actinin whole-cell staining was set as the target area, and the DAPI-stained nuclei were then extracted from each target area to determine the number of nuclei per target area. Then, MacroCellCount was performed, applying the settings from the reference picture to each picture from one set of experiment. The results were manually filtered for the following criteria: (a) 100 μm^2 < target area in micrometers squared < 3,000 μm^2 (size filter), (b) extraction from target area = 1 (1 nucleus filter), and (c) area ratio < 30% (cell surface to nucleus ratio filter). Statistical analyses were performed using SigmaPlot (version 11.0; Systat Software, Inc.). Equal distribution of the data was tested by Shapiro–Wilk test. The samples were then compared by Kruskal–Wallis test (one-way analysis of variance [ANOVA] on ranks). $n \geq 400$ (each condition, depending on the cell density).

Reporter gene assays

All the reporter gene assays shown in this study are performed in NRVCMs. Cells were infected with combinations of viruses expressing Dysbindin (20 ifu or 5, 10, 20, and 40 ifu for a dose-dependent experiment), 20 ifu Myozap, 10 ifu RhoA, and LacZ or GFP (as control or a filler virus to maintain equal count of viruses) along with adenovirus Ad-SRF-RE–luciferase (10 ifu) carrying a firefly luciferase and Ad-Renilla-luciferase carrying Renilla luciferase (for normalization of the measurements). For Dysbindin knockdown experiments, NRVCMs were transfected with siRNA against Dysbindin or control siRNA in addition to virus infection. In experiments of MEK1 inhibitor treatment, NRVCMs were simultaneously treated with MEK1 inhibitor during viral infection. Experiments were performed using a dual luciferase reporter assay kit (Promega), according to the manufacturer's instructions. Chemiluminescence was measured photometrically on an Infinite M200 PRO system (Tecan). All the experiments were performed in triplicate, quadruplicate, or hexaplicate and repeated two to three times.

Expression and purification of recombinant C3 transferase

Clostridium botulinum–derived exoenzyme C3 transferase (wild type) and its point mutant C3-E174Q (glutamate to glutamine at aa 174) were cloned in the plasmid pGEX-2T (GE Healthcare) and expressed as recombinant GST fusion proteins in *Escherichia coli* TG1 as described previously (Höltje et al., 2005). In brief, bacterial culture was grown at 37°C in 1 liter Luria Bertani medium (BD) containing 100 µg/ml ampicillin (Sigma-Aldrich) to an optical density of 0.7 at 595 nm. Culture was then supplemented with IPTG (Sigma-Aldrich) to a final concentration of 0.2 mM and incubated at 37°C for another 3 h. Bacteria were centrifuged at 7,700 *g* for 15 min (4°C) and resuspended in 20 ml lysis buffer containing 50 mM Tris, pH 8, 150 mM NaCl, 2 mM $MgCl_2$, and 2 mM DTT supplemented with protease

inhibitor cocktail (EDTA free; Roche). Bacteria were lysed by a French pressure cell press system (SIM-Aminco; Spectronic Instruments), and the suspension was centrifuged at 12,000 *g* for 15 min (4°C). The supernatant was incubated for 4 h at 4°C in 4 ml lysis buffer with 50% slurry of glutathione–Sepharose 4B beads (GE Healthcare). After incubation, slurry was subjected to a disposable chromatography column (Econo-Pac; Bio-Rad Laboratories), washed five times with ∼10 bed volumes of lysis buffer. Beads were incubated for 12 h at 4°C with 5 NIH U thrombin (GE Healthcare) to cleave of the GST tag. Finally, cleaved protein was eluted with 12 ml lysis buffer. Thrombin was removed by precipitation with benzamidine–Sepharose beads (AP Bioscience, LLC) and centrifuged at 500 *g* (10 min at room temperature). Buffer of the supernatant was then exchanged to 20 mM Hepes, pH 7.5, using PD-10 columns (Bio-Rad Laboratories) filtered through 0.22-µm filters and used for the cell culture experiments as indicated. ADP-ribosyltransferase activity was measured by an in vitro ADP-ribosylation assay described in the following paragraph.

ADP-ribosylation assay

2 µM GST-RhoA was incubated with wild-type or mutant C3 transferase protein at various concentrations and 1 µCi [^{32}P]NAD$^+$ (GE Healthcare) in 20 µl of 4× buffer containing 50 mM Hepes, pH 7.3, 10 mM $MgCl_2$, 10 mM DTT, 10 mM thymidine, and 10 mM NAD$^+$ (37°C for 20 min). The reaction was terminated by addition of Laemmli sample buffer and then incubated at 95°C for 10 min. Samples were resolved by SDS-PAGE on 15% gels, and the ADP-ribosylated RhoA was analyzed by phosphorimaging (Packard Cyclone; American Instrument).

RhoA and MEK1 inhibitor treatment and siRNA-mediated knockdown of Dysbindin

To inhibit the activation of RhoA or ERK1/2, NRVCMs were treated with Rho inhibitor C3 transferase (tebu-bio), C3 transferase, and E174Q mutant (recombinant purified protein; 1 µM) or MEK1 inhibitor PD98059 (New England Biolabs, Inc.) as per the manufacturer's instructions. Knockdown of Dysbindin expression was achieved by using Dysbindin siRNA (Santa Cruz Biotechnology, Inc.). Control siRNA-A, a nontargeting 20–25-nucleotide siRNA, was used as a negative control (Santa Cruz Biotechnology, Inc.). Knockdown of Dysbindin was confirmed by qRT-PCR or by immunoblotting.

Stimulation of hypertrophy in NRVCMs

Two distinct methods were applied to induce hypertrophy in NRVCMs, either by mechanical stretch or by application of pharmacological agent. Stretch-mediated hypertrophy was induced as reported earlier (Frank et al., 2012). In brief, NRVCMs were seeded at 10^7 cells/well in 0.25-mm transparent silicone membrane 6-well plates (Specialty Manufacturing), coated with 0.1 mg/ml collagen type I solution (Sigma-Aldrich), in DMEM containing 10% FCS, penicillin/streptomycin, and L-glutamine. After 24 h, cells were washed with PBS and serum starved in DMEM medium for another 24 h until biaxial stretch was applied to a total of 112% for 48 h using a 60-mm biaxial stretch device composed of a CO_2 series incubator (SHEL LAB) and FlexLink FX5000T-FLK purchased from Dunn Labortechnik. Prohypertrophic pharmacological stimulation was performed with 50 µM (or otherwise stated in the text or respective figure legends) PE (Sigma-Aldrich) or 1 µM ET (Sigma-Aldrich). Nonstimulated and unstretched cardiomyocytes served as controls in the respective experiments.

RNA isolation and qRT- PCR

Total RNA was isolated from NRVCMs or mouse left ventricles using lysis reagent (QIAzol; QIAGEN) following the manufacturer's instructions. 1 µg DNA-free total RNA was transcribed into cDNA using the first strand cDNA synthesis kit (SuperScript III; Life Technologies). For qRT-PCR, the EXPRESS SYBR GreenER reagent (Life Technologies) was used in a real-time PCR system (CFX96; Bio-Rad Laboratories). Cycling conditions used for all the qRT-PCRs are 3 min at 95°C followed by 40 cycles of 15 s at 95°C and 45 s at 60°C, a common step for annealing and extension at which step data were collected. Rpl32 (for NRVCMs) or 18S ribosomal RNA gene (for mouse tissues) was used as an internal standard for normalization (Frank et al., 2008). All the experiments were performed in triplicate, quadruplicate, or hexaplicate and repeated two to three times.

Protein preparation

Mouse left ventricles were homogenized with a tissue separator (Ultra-Turrax) in radioimmunoprecipitation assay buffer containing 1.0 mM Tris, 5 mM EDTA, pH 7.5, 1% NP-40 (vol/vol), 0.5% sodium deoxycholate (wt/vol), 0.1% SDS (wt/vol), protease inhibitor cocktail tablets (Roche), and phosphatase inhibitor cocktails 2 and 3 (Sigma-Aldrich), whereas NRVCMs were lysed by two to three freeze–thaw cycles in erythrocyte lysis buffer containing 50 mM Hepes, pH 7.0, 250 mM sodium chloride, 1% NP-40, 5 mM EDTA, and a phosphatase inhibitor and protease inhibitor cocktail. Cell debris was removed by centrifugation, and protein concentration was determined photometrically by Bradford/bicinchoninic acid assay method (Bio-Rad Laboratories).

Immunoblotting

Protein samples were resolved by 10 or 12% SDS-PAGE, transferred to a nitrocellulose or PVDF membrane, and immunoblotted with the target-specific primary antibodies. The overnight application of primary antibodies was followed by incubation with a suitable HRP-coupled secondary antibody (1:10,000; Santa Cruz Biotechnology, Inc.). Finally, visualization was achieved using a chemiluminescence kit (GE Healthcare) and detected on an imaging system (FluorChem Q; Biozym). Quantitative densitometry analysis was performed using ImageJ version 1.46 software (National Institutes of Health).

Statistical analyses

All results are shown as the means ± SEM unless stated otherwise. Statistical analyses of the data were performed using two-tailed Student's *t* test. When necessary, two-way ANOVA (followed by Student–Newman–Keuls post-hoc tests when appropriate) was applied. P-values of less than 0.05 were considered statistically significant.

Online supplemental material

Fig. S1 shows tissue distribution and subcellular localization of Dysbindin. Fig. S2 shows the effect of Dysbindin overexpression and knockdown on SRF signaling in cardiomyocytes. Fig. S3 shows the expression of Dysbindin in in vitro and in vivo models of hypertrophy and/or cardiomyopathy. Fig. S4 shows the effect of C3 transferase and its point mutant E174Q on cell surface area. Table S1 provides primers used for the cloning of full-length or different fragments of mouse Dysbindin. Online supplemental material is available at http://www.jcb.org/cgi/content/full/jcb.201303052/DC1. Additional data are available in the JCB DataViewer at http://dx.doi.org/10.1083/jcb.201303052.dv.

Y2H screening was performed at the protein interaction unit of the Genomics and Proteomics Core Facility at German Cancer Research Center (Heidelberg, Germany). We thank Gabriele Brunke, Katharina Stiebeling, and Vanessa Mangels for their excellent technical assistance. We also thank S. Schütze of the Department of Immunology (Christian-Albrechts University of Kiel) for the use of confocal microscope facility.

A.Y. Rangrez received a Young Investigator Grant from the Faculty of Medicine, Christian-Albrechts University of Kiel (Kiel, Germany). N. Frey was supported by grants from the Bundesministerium für Bildung und Forschung/National Genome Research Network-plus.

Submitted: 11 March 2013
Accepted: 22 October 2013

References

Allen, N.C., S. Bagade, M.B. McQueen, J.P. Ioannidis, F.K. Kavvoura, M.J. Khoury, R.E. Tanzi, and L. Bertram. 2008. Systematic meta-analyses and field synopsis of genetic association studies in schizophrenia: the SzGene database. *Nat. Genet.* 40:827–834. http://dx.doi.org/10.1038/ng.171

Benson, M.A., S.E. Newey, E. Martin-Rendon, R. Hawkes, and D.J. Blake. 2001. Dysbindin, a novel coiled-coil-containing protein that interacts with the dystrobrevins in muscle and brain. *J. Biol. Chem.* 276:24232–24241. http://dx.doi.org/10.1074/jbc.M010418200

Benson, M.A., C.L. Tinsley, and D.J. Blake. 2004. Myospryn is a novel binding partner for dysbindin in muscle. *J. Biol. Chem.* 279:10450–10458. http://dx.doi.org/10.1074/jbc.M312664200

Boerries, M., P. Most, J.R. Gledhill, J.E. Walker, H.A. Katus, W.J. Koch, U. Aebi, and C.A. Schoenenberger. 2007. Ca2+ -dependent interaction of S100A1 with F1-ATPase leads to an increased ATP content in cardiomyocytes. *Mol. Cell. Biol.* 27:4365–4373. http://dx.doi.org/10.1128/MCB.02045-06

Bray, N.J., A. Preece, N.M. Williams, V. Moskvina, P.R. Buckland, M.J. Owen, and M.C. O'Donovan. 2005. Haplotypes at the dystrobrevin binding protein 1 (DTNBP1) gene locus mediate risk for schizophrenia through reduced DTNBP1 expression. *Hum. Mol. Genet.* 14:1947–1954. http://dx.doi.org/10.1093/hmg/ddi199

Frank, D., C. Kuhn, B. Brors, C. Hanselmann, M. Lüdde, H.A. Katus, and N. Frey. 2008. Gene expression pattern in biomechanically stretched cardiomyocytes: evidence for a stretch-specific gene program. *Hypertension*. 51:309–318. http://dx.doi.org/10.1161/HYPERTENSIONAHA.107.098046

Frank, D., R. Frauen, C. Hanselmann, C. Kuhn, R. Will, J. Gantenberg, L. Füzesi, H.A. Katus, and N. Frey. 2010. Lmcd1/Dyxin, a novel Z-disc associated LIM protein, mediates cardiac hypertrophy in vitro and in vivo. *J. Mol. Cell. Cardiol.* 49:673–682. http://dx.doi.org/10.1016/j.yjmcc.2010.06.009

Frank, D., J. Gantenberg, I. Boomgaarden, C. Kuhn, R. Will, K.U. Jarr, M. Eden, K. Kramer, M. Luedde, H. Mairbäurl, et al. 2012. MicroRNA-20a inhibits stress-induced cardiomyocyte apoptosis involving its novel target Egln3/PHD3. *J. Mol. Cell. Cardiol.* 52:711–717. http://dx.doi.org/10.1016/j.yjmcc.2011.12.001

Frey, N., and E.N. Olson. 2003. Cardiac hypertrophy: the good, the bad, and the ugly. *Annu. Rev. Physiol.* 65:45–79. http://dx.doi.org/10.1146/annurev.physiol.65.092101.142243

Heineke, J., and J.D. Molkentin. 2006. Regulation of cardiac hypertrophy by intracellular signalling pathways. *Nat. Rev. Mol. Cell Biol.* 7:589–600. http://dx.doi.org/10.1038/nrm1983

Höltje, M., A. Hoffmann, F. Hofmann, C. Mucke, G. Grosse, N. Van Rooijen, H. Kettenmann, I. Just, and G. Ahnert-Hilger. 2005. Role of Rho GTPase in astrocyte morphology and migratory response during in vitro wound healing. *J. Neurochem.* 95:1237–1248. http://dx.doi.org/10.1111/j.1471-4159.2005.03443.x

Holzfeind, P.J., H.J. Ambrose, S.E. Newey, R.A. Nawrotzki, D.J. Blake, and K.E. Davies. 1999. Tissue-selective expression of alpha-dystrobrevin is determined by multiple promoters. *J. Biol. Chem.* 274:6250–6258. http://dx.doi.org/10.1074/jbc.274.10.6250

Kuwahara, K., and K. Nakao. 2011. New molecular mechanisms for cardiovascular disease:transcriptional pathways and novel therapeutic targets in heart failure. *J. Pharmacol. Sci.* 116:337–342. http://dx.doi.org/10.1254/jphs.10R28FM

Li, W., Q. Zhang, N. Oiso, E.K. Novak, R. Gautam, E.P. O'Brien, C.L. Tinsley, D.J. Blake, R.A. Spritz, N.G. Copeland, et al. 2003. Hermansky-Pudlak syndrome type 7 (HPS-7) results from mutant dysbindin, a member of the biogenesis of lysosome-related organelles complex 1 (BLOC-1). *Nat. Genet.* 35:84–89. http://dx.doi.org/10.1038/ng1229

Lien, C.F., C. Vlachouli, D.J. Blake, J.P. Simons, and D.C. Górecki. 2004. Differential spatio-temporal expression of alpha-dystrobrevin-1 during mouse development. *Gene Expr. Patterns*. 4:583–593. http://dx.doi.org/10.1016/j.modgep.2004.01.015

Miano, J.M. 2010. Role of serum response factor in the pathogenesis of disease. *Lab. Invest.* 90:1274–1284. http://dx.doi.org/10.1038/labinvest.2010.104

Miano, J.M., N. Ramanan, M.A. Georger, K.L. de Mesy Bentley, R.L. Emerson, R.O. Balza Jr., Q. Xiao, H. Weiler, D.D. Ginty, and R.P. Misra. 2004. Restricted inactivation of serum response factor to the cardiovascular system. *Proc. Natl. Acad. Sci. USA*. 101:17132–17137. http://dx.doi.org/10.1073/pnas.0406041101

Nelson, T.J., R. Balza Jr., Q. Xiao, and R.P. Misra. 2005. SRF-dependent gene expression in isolated cardiomyocytes: regulation of genes involved in cardiac hypertrophy. *J. Mol. Cell. Cardiol.* 39:479–489. http://dx.doi.org/10.1016/j.yjmcc.2005.05.004

Numakawa, T., Y. Yagasaki, T. Ishimoto, T. Okada, T. Suzuki, N. Iwata, N. Ozaki, T. Taguchi, M. Tatsumi, K. Kamijima, et al. 2004. Evidence of novel neuronal functions of dysbindin, a susceptibility gene for schizophrenia. *Hum. Mol. Genet.* 13:2699–2708. http://dx.doi.org/10.1093/hmg/ddh280

Parlakian, A., D. Tuil, G. Hamard, G. Tavernier, D. Hentzen, J.P. Concordet, D. Paulin, Z. Li, and D. Daegelen. 2004. Targeted inactivation of serum response factor in the developing heart results in myocardial defects and embryonic lethality. *Mol. Cell. Biol.* 24:5281–5289. http://dx.doi.org/10.1128/MCB.24.12.5281-5289.2004

Parlakian, A., C. Charvet, B. Escoubet, M. Mericskay, J.D. Molkentin, G. Gary-Bobo, L.J. De Windt, M.A. Ludosky, D. Paulin, D. Daegelen, et al. 2005. Temporally controlled onset of dilated cardiomyopathy through disruption of the SRF gene in adult heart. *Circulation*. 112:2930–2939.

Pieperhoff, S., S. Rickelt, H. Heid, W.C. Claycomb, R. Zimbelmann, C. Kuhn, S. Winter-Simanowski, C. Kuhn, N. Frey, and W.W. Franke. 2012. The plaque protein myozap identified as a novel major component of adhering junctions in endothelia of the blood and the lymph vascular systems. *J. Cell. Mol. Med.* 16:1709–1719. http://dx.doi.org/10.1111/j.1582-4934.2011.01463.x

Rees, M.L., C.F. Lien, and D.C. Górecki. 2007. Dystrobrevins in muscle and non-muscle tissues. *Neuromuscul. Disord.* 17:123–134. http://dx.doi.org/10.1016/j.nmd.2006.11.003

Rickelt, S., C. Kuhn, S. Winter-Simanowski, R. Zimbelmann, N. Frey, and W.W. Franke. 2011. Protein myozap—a late addition to the molecular ensembles of various kinds of adherens junctions. *Cell Tissue Res.* 346:347–359. http://dx.doi.org/10.1007/s00441-011-1281-8

Sanna, B., O.F. Bueno, Y.S. Dai, B.J. Wilkins, and J.D. Molkentin. 2005. Direct and indirect interactions between calcineurin-NFAT and MEK1-extracellular signal-regulated kinase 1/2 signaling pathways regulate cardiac gene expression and cellular growth. *Mol. Cell. Biol.* 25:865–878. http://dx.doi.org/10.1128/MCB.25.3.865-878.2005

Schwab, S.G., M. Knapp, S. Mondabon, J. Hallmayer, M. Borrmann-Hassenbach, M. Albus, B. Lerer, M. Rietschel, M. Trixler, W. Maier, and D.B. Wildenauer. 2003. Support for association of schizophrenia with genetic variation in the 6p22.3 gene, dysbindin, in sib-pair families with linkage and in an additional sample of triad families. *Am. J. Hum. Genet.* 72:185–190. http://dx.doi.org/10.1086/345463

Seeger, T.S., D. Frank, C. Rohr, R. Will, S. Just, C. Grund, R. Lyon, M. Luedde, M. Koegl, F. Sheikh, et al. 2010. Myozap, a novel intercalated disc protein, activates serum response factor-dependent signaling and is required to maintain cardiac function in vivo. *Circ. Res.* 106:880–890. http://dx.doi.org/10.1161/CIRCRESAHA.109.213256

Shore, P., and A.D. Sharrocks. 1995. The MADS-box family of transcription factors. *Eur. J. Biochem.* 229:1–13. http://dx.doi.org/10.1111/j.1432-1033.1995.tb20430.x

Straub, R.E., Y. Jiang, C.J. MacLean, Y. Ma, B.T. Webb, M.V. Myakishev, C. Harris-Kerr, B. Wormley, H. Sadek, B. Kadambi, et al. 2002. Genetic variation in the 6p22.3 gene DTNBP1, the human ortholog of the mouse dysbindin gene, is associated with schizophrenia. *Am. J. Hum. Genet.* 71:337–348. http://dx.doi.org/10.1086/341750

Strohmaier, J., J. Frank, J.R. Wendland, J. Schumacher, R.A. Jamra, J. Treutlein, V. Nieratschker, R. Breuer, M. Mattheisen, S. Herms, et al. 2010. A reappraisal of the association between Dysbindin (DTNBP1) and schizophrenia in a large combined case-control and family-based sample of German ancestry. *Schizophr. Res.* 118:98–105. http://dx.doi.org/10.1016/j.schres.2009.12.025

Talbot, K., W.L. Eidem, C.L. Tinsley, M.A. Benson, E.W. Thompson, R.J. Smith, C.G. Hahn, S.J. Siegel, J.Q. Trojanowski, R.E. Gur, et al. 2004. Dysbindin-1 is reduced in intrinsic, glutamatergic terminals of the hippocampal formation in schizophrenia. *J. Clin. Invest.* 113:1353–1363.

Talbot, K., N. Louneva, J.W. Cohen, H. Kazi, D.J. Blake, and S.E. Arnold. 2011. Synaptic dysbindin-1 reductions in schizophrenia occur in an isoform-specific manner indicating their subsynaptic location. *PLoS ONE*. 6:e16886. http://dx.doi.org/10.1371/journal.pone.0016886

Wilkins, B.J., Y.S. Dai, O.F. Bueno, S.A. Parsons, J. Xu, D.M. Plank, F. Jones, T.R. Kimball, and J.D. Molkentin. 2004. Calcineurin/NFAT coupling participates in pathological, but not physiological, cardiac hypertrophy. *Circ. Res.* 94:110–118. http://dx.doi.org/10.1161/01.RES.0000109415.17511.18

Zhang, X., G. Azhar, J. Chai, P. Sheridan, K. Nagano, T. Brown, J. Yang, K. Khrapko, A.M. Borras, J. Lawitts, et al. 2001a. Cardiomyopathy in transgenic mice with cardiac-specific overexpression of serum response factor. *Am. J. Physiol. Heart Circ. Physiol.* 280:H1782–H1792.

Zhang, X., J. Chai, G. Azhar, P. Sheridan, A.M. Borras, M.C. Furr, K. Khrapko, J. Lawitts, R.P. Misra, and J.Y. Wei. 2001b. Early postnatal cardiac changes and premature death in transgenic mice overexpressing a mutant form of serum response factor. *J. Biol. Chem.* 276:40033–40040. http://dx.doi.org/10.1074/jbc.M104934200